ISSN 0030-400X, Optics and Spectroscopy, 2017, Vol. 122, No. 3, pp. 420–425. © Pleiades Publishing, Ltd., 2017.

CONDENSED-MATTER SPECTROSCOPY

Temperature Dependent Surface and Spectral Modifications of Nano V_2O_5 Films[1]

M. Aslam Manthrammel[a, *], A. Fatehmulla[a, **], A. M. Al-Dhafiri[a], A. S. Alshammari[b], and Aslam Khan[c]

[a] *Department of Physics and Astronomy, College of Science, P. O. Box 2455, King Saud University, Riyadh 11451, Saudi Arabia*

[b] *Department of Physics, College of Science, University of Hail, P. O. Box 2440, Hail, Saudi Arabia*

[c] *King Abdullah Institute for Nanotechnology, King Saud University, Riyadh 11451, Saudi Arabia*

*e-mail: *muhd.aslam@gmail.com , **aman@ksu.edu.sa*

Received December 15, 2015; in final form, October 3, 2016

Abstract– Nanocrystalline V_2O_5 films have been deposited on glass substrates at 300°C substrate temperature using thermal evaporation technique and were subjected to thermal annealing at different temperatures 350, 400, and 550°C. X-ray diffraction (XRD) spectra exhibit sharper and broader characteristic peaks respectively indicating the rearrangement of nanocrystallite phases with annealing temperatures. Other phases of vanadium oxides started emerging with the rise in annealing temperature and the sample converted completely to VO_2 (B) phase at 550°C annealing. FESEM images showed an increase in crystallite size with 350 and 400°C annealing temperatures followed by a decrease in crystallite size for the sample annealed at 550°C. Transmission spectra showed an initial redshift of the fundamental band edge with 350 and 400°C while a blue shift for the sample annealed at 550°C, which was in agreement with XRD and SEM results. The films exhibited smart window properties as well as nanorod growth at specific annealing temperatures. Apart from showing the PL and defect related peaks, PL studies also supported the observations made in the transmission spectra.

DOI: 10.1134/S0030400X1703002X

INTRODUCTION

Transition metal oxides containing atoms with unfilled *d*-shells possess multiple oxidation states and exhibit the phenomenon of mixed valence. These properties make them suitable to subject for various chemical and structural transformations under the action of different external perturbations. These in turn are accompanied by significant modifications of the optical, electrical and other properties. Vanadium oxide thin films have attracted substantial interest among the transition metal oxide semiconductors as highly promising materials because of their wide range of striking properties [1, 2]. Varieties of techniques have been used to prepare vanadium oxide films. Among them, thermal evaporation [3], pulsed laser deposition (PLD) [4], magnetron sputtering [5], chemical vapor deposition (CVD) [6], spray pyrolysis [7] and sol–gel methods [8] are most commonly employed. Thermal evaporation method is of great interest due to its simple and easy to deposit nature, while the quality of the obtained films is mostly comparable with those prepared by the other processes. Among the vanadium oxide films, vanadium pentoxide (V_2O_5) thin films have attracted more attention due to their useful properties such as high chemical stability, electrochemical safety, low cost, easy preparation and relatively low toxicity [2].

Under reducing conditions, V_2O_5 films can be reduced to various oxide forms such as VO_2, V_2O_3 and mixed-valence phases (V_3O_7, V_4O_9, V_6O_{13}) where vanadium takes +III and +IV oxidation states [9–11]. Among them VO_2 films find broad applications because of their tunable electrical and optical properties. VO_2 exists in two phases – a non-thermochromic metastable polymorph phase VO_2 (B) and a thermochromic VO_2 (M/R) phase [12]. The latter is a thermotropic phase which exhibits switching behavior in electrical, optical and magnetic properties at its critical temperature $T_c = 68°C$ [1], and finds broad applications such as optical switching, smart window etc. It exhibits monoclinic phase below critical temperature T_c (represented by M) and a rutile phase above T_c (represented by R) and hence the name VO_2 (M/R) [13]. This phase has been extensively studied since its insulator/semiconductor-metal transition at about 68°C was discovered by Morin [11, 14]. The other phase (VO_2 (B)) of VO_2 films by reduction of V_2O_5 films pre-

[1] The article is published in the original.

Table 1. Crystallite size estimation of the as-deposited and isochronally annealed vanadium oxide films

Sample	2θ position	FWHM (β)	Crystallite size (D)
As-prepared	20.17°	0.356°	23 nm
350 °C annealed	40.56°	0.237°	36 nm
400 °C annealed	29.03°	0.091°	90 nm
550 °C annealed	28.72°	0.126°	65 nm

pared by thermal evaporation is far less investigated though it is simple and promising. Being a metastable phase, it can irreversibly be converted to the VO_2(M/R) phase by annealing in an inert atmosphere [15]. There are many recent studies on semiconducting VO_2 (B) polymorph in the form of nanorods and powders synthesized by thermal oxidation of vanadium and hydrothermal technique [16, 17]. Other techniques include sputtering, evaporation, sol–gel process, pulsed laser deposition etc. [1, 18–20].

In this work, we present growth and characterization of V_2O_5 thin films by thermal evaporation technique and its reduction to VO_2 phase by simple thermal annealing process. The investigations include observations of smart material properties as well as nanorod growth.

EXPERIMENTAL

Thin films of V_2O_5 have been deposited by thermal evaporation in a vacuum deposition chamber (Hindhivac vacuum coating unit) on top of BSG substrates. The source material, pure V_2O_5 has been evaporated from a molybdenum boat. The deposition pressure inside the chamber has been maintained between 8×10^{-6} and 4×10^{-5} mbar and the source–substrate distance has been kept at approximately 14 cm. Since the films prepared at lower substrate temperatures are amorphous in nature [21], the films are deposited at a constant substrate temperature (300°C). Post annealing has been performed on the deposited films at temperatures 350, 400 and 550°C, respectively, for 1 hour in air using Eurotherm tube furnace from Carbolite, Sheffield, England.

The structural properties of the prepared films (both as-deposited and post-annealed) have been determined by X-ray diffraction (XRD) using a PANalytical X'Pert PRO with Cu Kα radiation at 45 kV and 40 mA. Surface morphology has been carried out using JEOL (JSM-7600F) field emission scanning electron microscope. Optical measurements have been performed using a Varian Carry 5000 spectrophotometer (UV-Vis-NIR). Photoluminescence (PL) studies were carried out using a HORIBA Scientific Fluoromax-4P spectrofluorometer.

RESULTS AND DISCUSSION

X-ray diffraction patterns were recorded to explore the phase purity and crystallinity before and after annealing the V_2O_5 film. Figure 1a shows the XRD analysis of as-deposited as well as isochronally annealed vanadium oxide thin films. The as-deposited thin film is crystallized in purely orthorhombic V_2O_5 phase and matches well with the ICDD file # 01-077-2418. As we anneal the sample above 350°C, VO_2 phase slowly started emerging and finally crystallized in pure monoclinic VO_2 phase (ICDD# 01-071-0042) at 550°C annealing temperature. The orientation peak (001) of V_2O_5 gradually changes to (002) peak of VO_2 at 400°C annealing. The film also contains V_3O_5 (ICDD# 01-071-0039) and V_7O_3 (ICDD# 00-030-1425) at 400°C. The film annealed at 550°C has distinctly different peaks than the other patterns. At 550°C the sample completely converts to VO_2 phase as depicted in the Fig. 1a. This phase is identified as VO_2 (B) polymorph. The orientation peak has shifted to (−202) peak of monoclinic VO_2 at 550°C.

In order to observe the peak positions more distinctly, the selective peaks have been redrawn at specific 2θ positions as shown in Figs. 1b, 1c. In Fig. 1b an explicit peak shift towards left can be observed for the peak at 29.06° for the sample annealed at 550°C indicating the formation of (−202) plane of VO_2. Similar observations were noticed for the peaks corresponding to (211), (401) and (311) planes of V_2O_5 in Fig. 1c. However, here the shift is towards right. At 550°C the sample has been completely converted to VO_2 phase and the corresponding planes have been marked.

The crystallite size based on the orientation peaks have been determined using Scherrer formula and tabulated in Table 1. The table shows an overall increase in crystallite size with the increase in annealing temperature. However, the sample annealed at 550°C provided an opposite trend giving 65 nm crystallite size, though the crystallite size has been increased individually. In order to understand this observations more clearly SEM analysis and optical studies of the samples were carried out.

Figure 2 shows the FESEM images of the as-deposited as well as isochronally annealed vanadium oxide thin films. It is observed that the as-deposited V_2O_5 film shown in Fig. 2a displays uniformly distributed small identical grains. It is characteristic behavior of either amorphous film or nanocrystalline film. XRD analysis indicates that the sample growth is that of orthorhombic nano V_2O_5 structure. Figure 2b shows the morphological changes occurred during the annealing process at 350°C. This resulted in larger crystallites with more granular and micro-cracked surface [1]. The sample annealed at 400°C in Fig. 2c shows a larger distribution of grains with very ordered growth. A low magnified image of the same sample

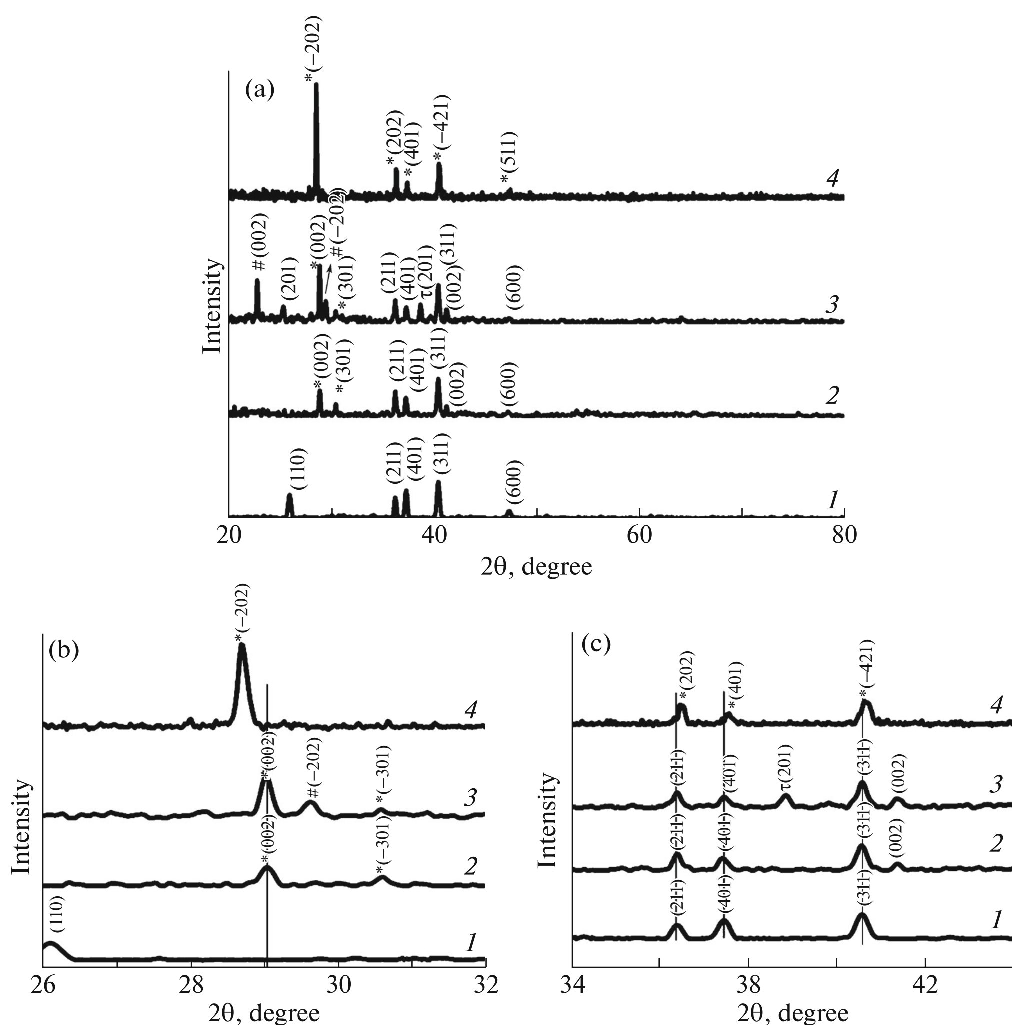

Fig. 1. (a) XRD analysis of as-deposited and isochronally annealed films: V_2O_5: 01-077-2418, *—VO_2 : 01-071-0042, τ—V_3O_5: 01-071-0039, #—V_7O_3: 00-030-1425; (b, c) XRD pattern depicting the shift in 2θ position for the vanadium oxide films: as-deposited (*1*), annealed at 350 (*2*), 400 (*3*), 550°C (*4*).

(inset of Fig. 2c) shows that there is a multi-aligned nanorod-like growth of crystallites for this film [2, 21]. The sample annealed at 550°C (shown in Fig. 2d) shows a comparatively larger crystallite size distribution than that of as-deposited and sample annealed at 350°C, but smaller than that of 400°C annealed sample. However, the sample displayed a more ordered growth with valleys and agglomeration of identical crystallites [22].

The optical transmittance spectra of isochronally annealed V_2O_5 films at different temperatures in the UV–vis-NIR range is shown in Fig. 3a. From the figure, as-deposited sample shows two ripples with a fundamental band edge around 490 nm. As the annealing temperature increases, the ripples slowly disappear indicating the surface modification and reducing the thickness of the thin film. In order to estimate the thickness of the film, the transmission data was simulated and fitted using the method described by Birgin et al. [23]. The thicknesses of the films obtained were 220, 130, 108, and 92 nm for the as-deposited film, films annealed at 350, 400, and 550°C, respectively. This decrease in the film thickness may be due to the reaction of the ambient molecules with the oxygen contained in the V_2O_5 film resulting in the reduction of the vanadium oxide and partial removal or rearrangement of the microstructure. It was observed that the annealing treatment greatly influenced the transmission of the film. The color of the film changed from yellow to dark yellow at 400°C annealing temperature. However, at 550°C annealing temperature it was comparatively light yellow with improved transmission. The transmission spectra clearly justify this observation. From the spectra it is evident that as-deposited V_2O_5 film exhibits significant transmission covering the whole spectral region starting from the IR to the visible. The sample annealed at 350°C exhibits good transmittance in the visible region while the

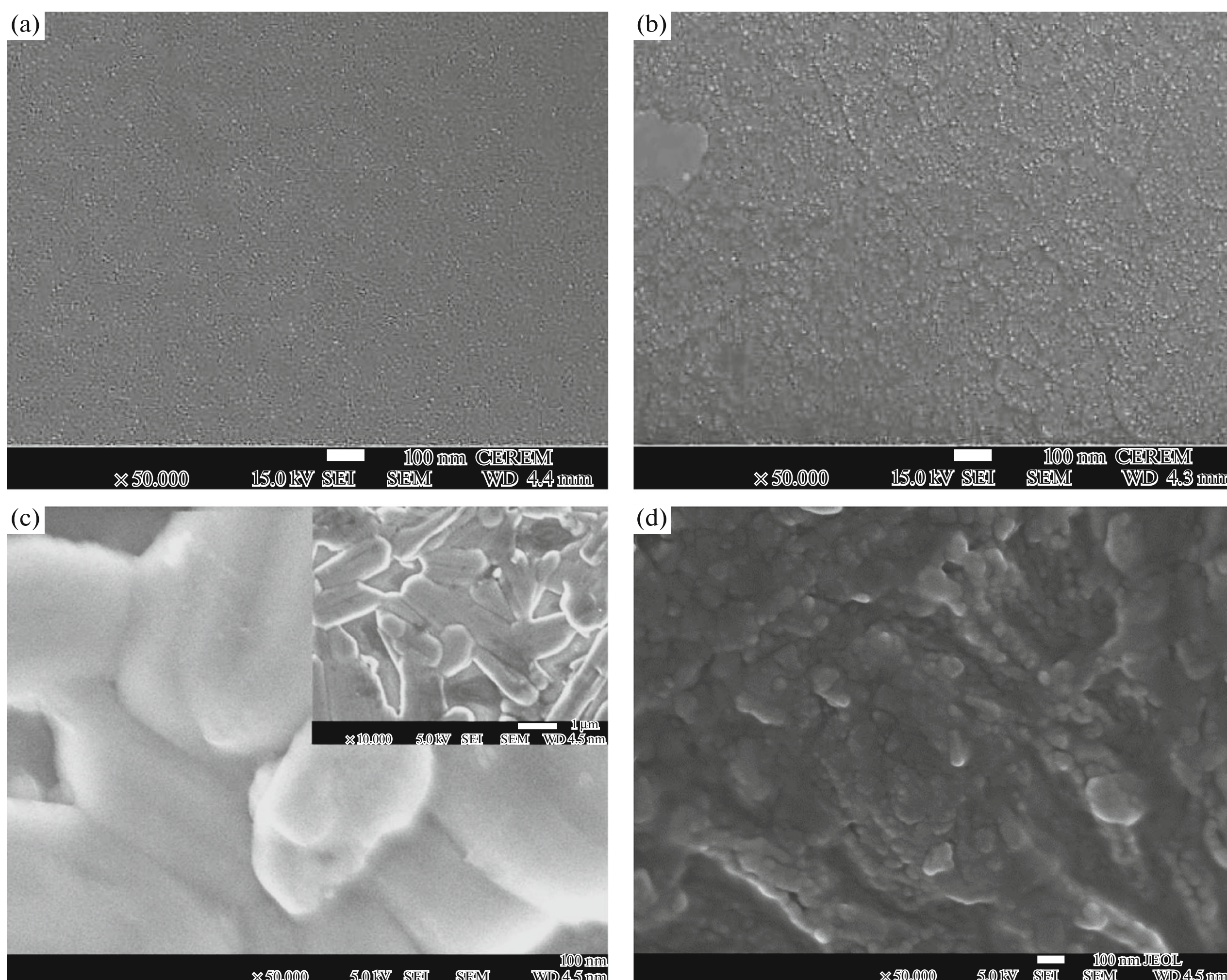

Fig. 2. FESEM images of the vanadium oxide films: as-deposited (a), annealed at 350 (b), 400 (c), 550°C (d). Low magnification (10000×) FESEM image of the vanadium oxide film annealed at 400°C is shown as inset of (c).

transmittance is diminishing in the IR region making it a potential choice as a smart window material. The sample annealed at 550°C shows improved transmission characteristics compared to other annealed samples in the entire range from UV to IR.

Figure 3b shows the Tauc's plot for the as-deposited and isochronally annealed vanadium oxide films. The value of band gap for the pure V_2O_5 was reported as 2.2–2.4 eV [24, 25]. The optical band gap values for the direct transition are tabulated in Table 2.

Table 2. Band gap calculation from Tauc's plot

Film	Band gap, eV	Corresponding wavelength, nm
As-deposited	2.54	490
Annealed at 350°C	2.42	513
Annealed at 400°C	1.88	660
Annealed at 550°C	3.40	365

Optical band gap values are slightly higher than the reported value, which is due to the nanocrystalline growth of the film [26]. As-deposited V_2O_5 sample gives a direct band gap of 2.54 eV corresponding to 490 nm wavelength. As the annealing temperature increased, the band gap values started decreasing giving a clear red shift. For the samples annealed at 350 and 400°C the band gap values are found to be 2.42 and 1.88 eV, respectively. This is in accordance with the previous reports on annealing the thin film samples and can be attributed to the microstructural changes caused by annealing treatment, i.e., increase in the crystallite size with increase in annealing temperature [2, 27]. The energy gap between valence band and conduction band decreases with the increase of crystallite size [28]. However, a clear blue shift of band gap from 2.54 to the 3.40 eV was observed for the sample annealed at 550°C. Though rare this indeed hap-

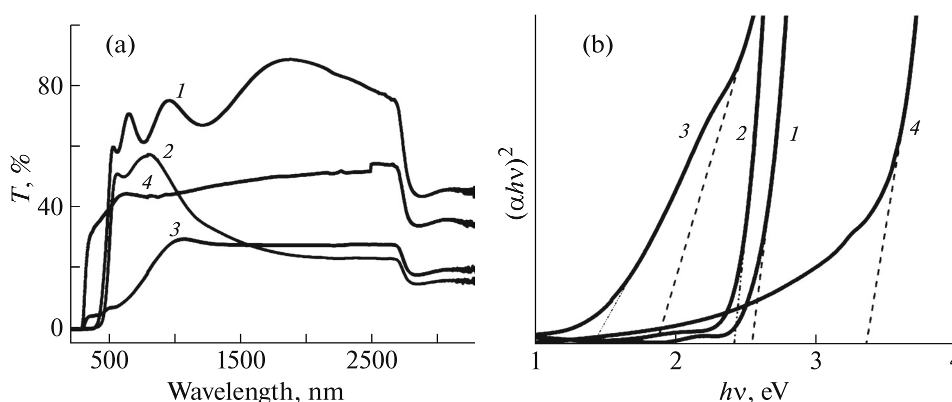

Fig. 3. (a) Transmission spectra and (b) Tauc's plots of as-deposited and isochronally annealed V_2O_5 films: as-grown (*1*), annealed at 350 (*2*), 400 (*3*), 550°C (*4*).

pens in thin films at higher temperatures and could be explained predominantly by means of Burstein-Moss bandgap widening effect suggesting unusual absence of band narrowing effect [7, 29–32]. Burstein-Moss effect result in pushing the Fermi level up and block the excitation from the valence band to these occupied lowest states below Fermi level, thereby causing band gap widening and resulting in a blue shift of the absorption edge. This band gap widening is responsible also for the enhanced transmission in the UV region for the sample annealed at 550°C in Fig. 3a [7]. This sample showed a better transmittance than other annealed samples which confirms the increase of carrier concentration and Burstein-Moss effect.

Figure 4 shows PL emission spectra of as-deposited and isochronally annealed films at excitation wavelength 300 nm measured using a HORIBA Scientific Fluoromax-4P spectrofluorometer. The spectra show good luminescence with series of bands. Prominent band is observed at green yellow region of the spectrum, centered at 570 nm. The PL peaks observed at violet region centered at 407 nm may be due to a defect level which might be associated with the incorporation of oxygen vacancies during nanostructured evolution [33, 34]. A weak emission band at blue region centered at 466 nm slowly develops with the annealing temperature [35]. The peak observed at 490 nm for the as-deposited film is attributed to the band-to-band transition of V_2O_5 film while the corresponding peaks are marked at 328 and 368 nm for the films annealed at 400 and 550°C, respectively. It was also noted that a band once formed continued to appear even after the treatment or structural change. Moreover, with the same argument the very weak PL peak observed at 552 nm is attributed to the band to band transition carried from the bulk V_2O_5 [36].

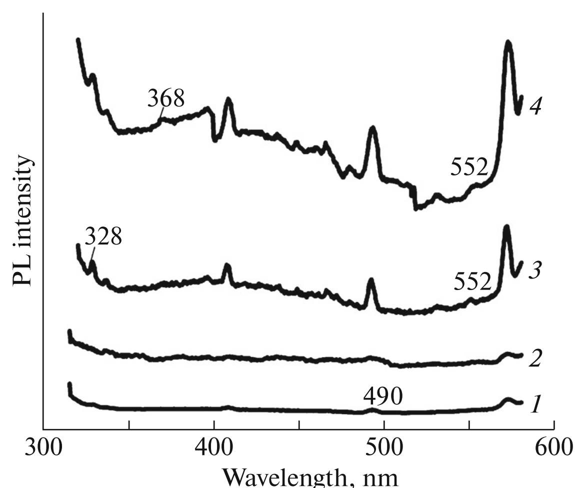

Fig. 4. Photoluminescence spectra of as-deposited and isochronally annealed vanadium oxide films excited at 300 nm: as-grown (*1*), annealed at 350 (*2*), 400 (*3*), 550°C (*4*).

CONCLUSION

Highly ordered orthorhombic nano-V_2O_5 thin films were prepared on glass substrates at 300°C substrate temperature using thermal evaporation technique and subjected to thermal annealing. The structural, optical and morphological properties of the films showed strong dependence on the annealing temperature. XRD spectra showed rearrangement of nanocrystallite phases with temperature and reduction of V_2O_5 to VO_2 phase at higher temperatures. FESEM images also confirmed the observations in XRD analysis with an increasing crystallite size with annealing temperature from the 350°C to 400°C followed by a decrease in crystallite size at 550°C. The films annealed at 400°C exhibited an improved crystallinity and nanorods-like morphology. Thus controlled annealing in air can result in emergence of ordered nanorods and can be tailored for various applications. Transmission spectra was also in agreement with the above observations exhibiting an initial redshift of the

fundamental band edge with 350 and 400°C while a blue shift for the sample annealed at 550°C. The observed blue shift was explained predominantly by Moss-Burstein band gap widening effect. PL studies also supported the observations made in the transmission spectra. Therefore, thermal treatment demonstrates strong influence on crystallization process as well as optical properties of V_2O_5 films that can be tailored for suitable device applications.

ACKNOWLEDGMENTS

This project was supported by King Saud University, Deanship of Scientific Research, College of Science Research Center.

REFERENCES

1. O. Monfort, T. Roch, L. Satrapinskyy, M. Gregor, T. Plecenik, A. Plecenik, and G. Plesch, Appl. Surf. Sci. **322**, 21 (2014).
2. D. Vasanth Raj, N. Ponpandian, D. Mangalaraj, and C. Viswanathan, Mater. Sci. Semicond. Process. **16**, 256 (2013).
3. R. T. R. Kumar, B. Karunagaran, V. S. Kumar, Y. L. Jeyachandran, D. Mangalaraj, and S. K. Narayandass, Mater. Sci. Semicond. Process. **6**, 543 (2003).
4. Y. Iida, Y. Kaneko, and Y. Kanno, J. Mater. Process. Technol. **197**, 261 (2008).
5. A. C. M. Esther, D. Porwal, M. S. Pradeepkumar, D. Rangappa, A. K. Sharma, and A. Dey, Phys. B **478**, 161 (2015).
6. N. K. Nandakumar and E. G. Seebauer, Thin Solid Films **519**, 3663 (2011).
7. R. Irani, S. M. Rozati, and S. Beke, Mater. Chem. Phys. **139**, 489 (2013).
8. D. Alamarguy, J. E. Castle, N. Ibris, and A. M. Salvi, Surf. Interface Anal. **38**, 801 (2006).
9. M. C. Rao, Res. J. Recent Sci. **2**, 67 (2013).
10. D. S. Su and R. Schlögl, Catal. Lett. **83**, 115 (2002).
11. Y. Ningyi, L. Jinhua, and L. Chenglu, Appl. Surf. Sci. **191**, 176 (2002).
12. S. Chen, J. Lai, J. Dai, H. Ma, H. Wang, and X. Yi, Opt. Express **17**, 24153 (2009).
13. L. Chen, C. Huang, G. Xu, L. Miao, J. Shi, J. Zhou, and X. Xiao, J. Nanomater. **2012**, 8 (2012).
14. F. J. Morin, Phys. Rev. Lett. **3**, 34 (1959).
15. P. Kiri, G. Hyett, and R. Binions, Adv. Mater. Lett. **1**, 86 (2010).
16. A. Lafort, H. Kebaili, S. Goumri-Said, O. Deparis, R. Cloots, J. de Coninck, M. Voué, F. Mirabella, F. Maseri, and S. Lucas, Thin Solid Films **519**, 3283 (2011).
17. T. C. K. Yang, Y.-L. Yang, R.-C. Juang, T.-W. Chiu, and C.-C. Chen, Vacuum **121**, 310 (2015).
18. L. Xingxing, W. Shao-Wei, C. Feiliang, Y. Liming, and C. Xiaoshuang, J. Phys. D. **48**, 265104 (2015).
19. C.-C. Lin, Y. Hu, and J.-S. Liu, Int. J. Chem. Eng. Appl. **4**, 54 (2013).
20. Q. Shi, W. Huang, Y. Zhang, S. Qiao, J. Wu, D. Zhao, and J. Yan, J. Mater. Sci.: Mater. Electron. **23**, 1610 (2012).
21. M. Prześniak-Welenc, M. Łapiński, T. Lewandowski, B. Kościelska, L. Wicikowski, and W. Sadowski, J. Nanomater. **2015**, 1 (2015).
22. P. A. Premkumar, M. Toeller, I. P. Radu, C. Adelmann, M. Schaekers, J. Meersschaut, T. Conard, and S. V. Elshocht, ECS J. Solid State Sci. Technol. **1**, 169 (2012).
23. E. G. Birgin, I. Chambouleyron, and J. M. Martínez, J. Comput. Phys. **151**, 862 (1999).
24. D. W. Bullett, J. Phys. C **13**, L595 (1980).
25. J. Meyer, K. Zilberberg, T. Riedl, and A. Kahn, J. Appl. Phys. **110**, 033710 (2011).
26. M. M. Aslam, S. M. Ali, A. Fatehmulla, W. A. Farooq, M. Atif, A. M. Al-Dhafiri, and M. A. Shar, Mater. Sci. Semicond. Process. **36**, 57 (2015).
27. C. W. Zou, X. D. Yan, J. Han, R. Q. Chen, and W. Gao, J. Phys. D **42**, 145402 (2009).
28. T. Van Buuren, L. N. Dinh, L. L. Chase, W. J. Siekhaus, and L. J. Terminello, Phys. Rev. Lett. **80**, 3803 (1998).
29. J.-W. Jeon, D.-W. Jeon, T. Sahoo, M. Kim, J.-H. Baek, J. L. Hoffman, N. S. Kim, and I.-H. Lee, J. Alloy. Compd. **509**, 10062 (2011).
30. T. S. Moss, Proc. Phys. Soc. B **67**, 775 (1954).
31. E. Burstein, Phys. Rev. **93**, 632 (1954).
32. B. He, J. Xu, H. Xing, C. Wang, and X. Zhang, Superlatt. Microstruct. **64**, 319 (2013).
33. V. Petkov, P. Y. Zavalij, S. Lutta, M. S. Whittingham, V. Parvanov, and S. Shastri, Phys. Rev. B **69**, 085410 (2004).
34. Z. Zhang, Y. Zhao, and M. Zhu, Appl. Phys. Lett. **88**, 033101 (2006).
35. B. S. Acharya and B. B. Nayak, Indian J. Pure Appl. Phys. **46**, 866 (2008).
36. N. Kenny, C. R. Kannewurf, and D. H. Whitmore, J. Phys. Chem. Solids **27**, 1237 (1966).